



Contents lists available at ScienceDirect

Applied Surface Science

journal homepage: www.elsevier.com/locate/apsusc



Enhanced in vitro biocompatibility of ultrafine-grained biomedical NiTi alloy with microporous surface

C.Y. Zheng^{a,b,c}, F.L. Nie^{a,b,c}, Y.F. Zheng^{a,b,c,*}, Y. Cheng^c, S.C. Wei^{d,**}, R.Z. Valiev^e

^a State Key Laboratory for Turbulence and Complex System, College of Engineering, Peking University, Beijing 100871, China

^b Department of Advanced Materials and Nanotechnology, College of Engineering, Peking University, Beijing 100871, China

^c Center for Biomedical Materials and Tissue Engineering, Academy for Advanced Interdisciplinary Studies, Peking University, Beijing 100871, China

^d Department of Oral and Maxillofacial Surgery, School of Stomatology, Peking University, Beijing 100081, China

^e Institute of Physics of Advanced Materials, Ufa State Aviation Technical University, Ufa, Russia

ARTICLE INFO

Article history:

Received 5 April 2011

Received in revised form 24 May 2011

Accepted 25 May 2011

Available online xxx

Keywords:

Ultrafine-grained alloy

Surface modification

Corrosion resistance

Cytocompatibility

ABSTRACT

Bulk ultrafine-grained Ni_{50.8}Ti_{49.2} alloy (UFG-NiTi) was successfully fabricated by equal-channel angular pressing (ECAP) technique in the present study, and to further improve its surface biocompatibility, surface modification techniques including sandblasting, acid etching and alkali treatment were employed to produce either irregularly roughened surface or microporous surface or hierarchical porous surface with bioactivity. The effect of the above surface treatments on the surface roughness, wettability, corrosion behavior, ion release, apatite forming ability and cytocompatibility of UFG-NiTi alloy were systematically investigated with the coarse-grained NiTi alloy as control. The pitting corrosion potential (E_{pit}) was increased from 393 mV (SCE) to 704 mV (SCE) with sandblasting and further increased to 1539 mV (SCE) with following acid etching in HF/HNO₃ solution. All the above surface treatment increased the apatite forming ability of UFG-NiTi in varying degrees when soaked them in simulated body fluid (SBF). Meanwhile, both sandblasting and acid etching could promote the cytocompatibility for osteoblasts: sandblasting enhanced cell attachment and acid etching increased cell proliferation. The different corrosion behavior, apatite forming ability and cellular response of UFG-NiTi after different surface modifications are attributed to the topography and wettability of the resulting surface oxide layer.

© 2011 Elsevier B.V. All rights reserved.

1. Introduction

With the development of severe plastic deformation (SPD) techniques, ultrafine-grained metals with grain sizes in the range of 10–1000 nm have been developed, e.g. copper, iron, titanium and nitinol [1–3]. An enhanced pre-osteoblast [4], fibroblast [5] and stem cell [6] behaviors on ultrafine-grained titanium were reported. In addition, the yield tensile strength of ultrafine-grained titanium is higher than 950 MPa at a strain rate of 10⁻³ s⁻¹ and endurance of more than 500 MPa at 2 × 10⁷ cycles, meanwhile with excellent biological compatibility [1,7].

One of the authors in this study found that the ultrafine-grained NiTi demonstrated very high tensile strength up to 1400–1600 MPa and ductility of dozen percents during elongation at 300–600 °C

[3]. Recent work on ultrafine-grained NiTi fabricated by high pressure torsion (HPT) technique showed higher corrosion resistance and equivalent cytocompatibility either within L-929 or MG 63 culture compared with microcrystalline NiTi alloy by the present authors [8]. Compared to pure titanium, NiTi alloy with nearly equiatomic nickel and titanium contents has advantages of shape memory effect and superelasticity, and they were widely utilized as biomedical appliances in dentistry, orthopedics and interventional therapy.

However, the surfaces of both coarse-grained NiTi and ultrafine-grained NiTi are still bioinert by nature and cannot form a bioactive bond with the living bone if implanted in a bony site while bioactivity is required when used as bone implants such as intramedullary nails. Surface modification was thus employed to improve surface bioactivity and eliminate or reduce the adverse effect of nickel ion release.

Till now, little work has been done to endow ultrafine-grained metals with bioactivity for biomedical application. Micro-arc oxidation [9], grit-blasting [10], magnetron sputtering [11] and combined mechanical and chemical treatment [12] were employed to improve the surface biocompatibility of ultrafine-grained

* Corresponding author at: Department of Advanced Materials and Nanotechnology, College of Engineering, Peking University, Beijing 100871, China.
Tel.: +86 10 6276 7411; fax: +86 10 6276 7411.

** Co-corresponding author.

E-mail address: yfzheng@pku.edu.cn (Y.F. Zheng).

titanium. Ultrafine-grained austenitic stainless steel was coated with nanohydroxyapatite by electrodeposition [13] to achieve surface bioactivity, while ultrafine-grained NiTi was surface coated with a novel SrO–SiO₂–TiO₂ sol–gel coating to enhance its corrosion resistance and cellular behavior [14]. In the present study, irregularly roughened surface, microporous surface and hierarchical porous surface of ultrafine-grained NiTi were achieved by single step treatment of sandblasting or by duplex treatment of sandblasting and acid etching or three-step treatment of sandblasting with acid etching followed by alkaline treatment respectively. The effect of the above treatments on the *in vitro* biocompatibility of ultrafine-grained NiTi such as corrosion resistance, ions release, apatite forming ability and cellular behavior were studied systematically. The *in vitro* biocompatibility of ultrafine-grained NiTi is also studied in comparison with that of coarse-grained NiTi.

2. Materials and methods

2.1. Surface modification

Ultrafine-grained NiTi (50.8 at.% Ni, dubbed UFG-NiTi) was prepared by ECAP technique from commercial coarse-grained Ni_{50.8}Ti_{49.2} (dubbed CG-NiTi) discs (both provided by Ufa State Aviation Technical University) with subsequent anneal in vacuum at a temperature of 300 °C for 30 min. It has equiaxed grains with a mean grain size of 200–300 nm. Rectangular strips with typical dimensions of 10 mm × 10 mm × 1.5 mm were cut by spark-erosion wire cutting, ground with SiC paper up to 2000 grit, and cleaned ultrasonically in acetone for 10 min, in ethanol for 10 min and in distilled water for 10 min in turn, then dried at 40 °C in a dryer. Some of UFG-NiTi samples were sandblasted by 60 grit corundum particles at the pressure of 0.5 MPa (SB-NiTi) and then cleaned ultrasonically in acetone, ethanol and distilled water in turn for further chemical modification treatment: acid etching (AE-NiTi) and acid etching plus alkali treatment (AEAT-NiTi). AE-NiTi was performed by HF/HNO₃ solution etching consisting of 15 ml HNO₃ + 5 ml HF + 80 ml H₂O in ultrasonic bath for 1 min at room temperature of ~22 °C. AEAT-NiTi was etched in 40% HCl at 100 °C for 10 min, thereafter immersed in 1.5 M NaOH solution at 60 °C for 24 h. All the above treated samples were rinsed in distilled water and dried at 40 °C in a dryer.

2.2. Corrosion behavior

The electrochemical corrosion measurements were performed using an electrochemical workstation (CHI600C, China) at room temperature of ~22 °C. The electrolyte was simulated body fluid (SBF) proposed by Kokubo without organic species [15]. The ion concentrations are as follows: Na⁺ 142.0, K⁺ 5.0, Mg²⁺ 1.5, Ca²⁺ 2.5, HCO₃⁻ 4.2, Cl⁻ 147.8, HPO₄²⁻ 1.0, SO₄²⁻ 0.5 mM, which is nearly equal to those of human blood plasma except HCO₃⁻ being 27.0 mM. The sample was set as a working electrode, a platinum electrode acting as an auxiliary electrode and the reference electrode a saturated calomel electrode (SCE). The OCP (open circuit potential) measurement was maintained up to 7200s. Electrochemical impedance spectroscopy (EIS) was obtained with a sinusoidal wave of 10 mV in amplitude to the working electrode around OCP at a frequency range from 100 kHz to 10 mHz. Both potentiodynamic polarization curves and cyclic polarization curves were measured from -800 mV (vs. SCE) to 2000 mV (vs. SCE) with a scan rate of 1 mV/s.

Concerns about the potential risk associated with corrosion of NiTi alloy has been reported due to the biological side effects of Ni. Nickel ion release was measured by immersion test. NiTi alloy plates were immersed in SBF at 37 ± 0.5 °C for 28 days. The

inductively coupled plasma atomic emission spectrometry (Leeman, Profile ICP-AES) was utilized to determine the amount of Ni ions.

2.3. Apatite forming ability tests

The apatite forming ability of the surface modified UFG-NiTi alloy was evaluated by soaking in SBF. Each sample was incubated in 20 ml of SBF in a Teflon-sealed bottle for 3, 7, 14 days at 37 °C with solution changed every other day. After the above soaking, the samples were rinsed in distilled water and dried at 40 °C in a dryer.

2.4. Cell experiment

Cell adhesion and proliferation tests were performed with osteoblast-like cell line MG63 (CRL1427, ATCC, USA). Before performing these assays, the cells were cultured in MEM medium (Invitrogen) supplemented with 10% of fetal calf serum and 1% penicillin/streptomycin at 37 °C in a humidified atmosphere of 5% CO₂ in air. MG63 cells were seeded onto the CG-NiTi, UFG-NiTi, SB-NiTi, AE-NiTi, AEAT-NiTi samples in 24-well culture plates at a density of 5 × 10⁴ cells well⁻¹ for direct cell adhesion observation. After 4 h and 3 days incubation, the culture media were removed and specimens were fixed with 2.5% glutaraldehyde solution for 1 h at room temperature and rinsed 3 times with phosphate buffer solution (PBS, pH = 7.4), followed by dehydration in a gradient ethanol/distilled water mixture (50%, 60%, 70%, 80%, 90%, 100%) for 10 min and dried in air. Samples were sputter coated with gold for cell morphology observation using SEM.

For the evaluation of cell attachment, cells were cultured for 4 h and 24 h in 24-well culture plates at an initial seeding density of 5 × 10⁴ cells well⁻¹. After trypsinization of the attached cells, cell numbers were counted using a hemocytometer. Cell proliferation was determined using 3-(4,5-dimethylthiazol-2-yl)-2,5-diphenyltetrazolium bromide (MTT; Sigma) assay by a colorimetric assay. Cells were seeded at a concentration of 5 × 10⁴ cells well⁻¹ onto the sample in MEM under standard cell-culture condition described above. The control groups involved the use of MEM medium as negative control and MEM medium with 10% dimethylsulfoxide as positive control. The cells were harvested for the MTT assay at 3, 7 and 9 days. At each stage, 60 μl/well of MTT was added to each well and the cells were incubated for 4 h at 37 °C. Afterwards, 600 μl formazan solubilization solution (10% SDS in 0.01 M HCl) was added to each well for 12 h in the incubator in a humidified atmosphere. The spectrophotometrical absorbance of the samples was measured by microplate reader (Bio-RAD680) at 570 nm with a reference wavelength of 630 nm. Each experiment was performed in quadruple for each group and repeated twice.

2.5. Surface characterization

Before and after soaking in SBF, the surface morphology and composition of the surface modified UFG-NiTi alloy were assessed by scanning electron microscope (SEM, HITACHI S-4800) equipped with an energy dispersive spectrometer (EDS), and analyzed by X-ray photoelectron spectroscopy (XPS, AXIS-Ultra Instrument) and X-ray diffractometer (XRD) using a Rigaku DMAX 2400 diffractometer with Cu Kα irradiation. Before the SEM analysis, the specimen surfaces were coated with gold films. Surface wettability was tested by contact angle in quintuplicate. The image of the droplet was captured and the contact angle was measured using OCA20 drop shape analysis program (Dataphysics Instrument, Germany).

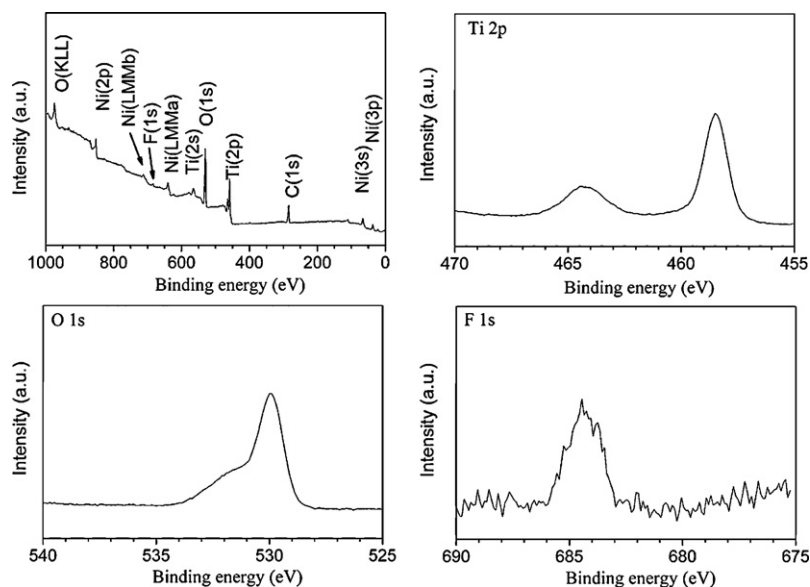


Fig. 3. XPS survey spectrum, Ti 2p, O 1s and F 1s spectra of AE-NiTi.

sandblasting. Meanwhile, microporous surface with pores ranging from several to tens of micrometers were yielded during etching (Fig. 1(c)). XPS results in Fig. 3 show that the outmost oxide film of AE-NiTi was TiO_2 , as evidenced by the binding energies of Ti 2p signal at 458.4 eV and O 1s signal at 530.2 eV [16]. Some fluorine was also incorporated during acid etching in HF/ HNO_3 solution. HCl etching plus NaOH treatment of UFG-NiTi samples resulted in hierarchical porous surface (Fig. 1(d)). There were concavities tens of micrometers in size with tens of nanometer-size pores uniformly distributed among them. XRD profiles show that the surface layer of AE-NiTi was mainly NiTi_2 while AEAT-NiTi had NiTi and $\text{Ti}_2\text{NiH}_{0.5}$ on their surfaces. Since EDS spectrum (Fig. 1(d)) evidenced the existence of titanium, nickel, sodium and oxygen elements on the surface of AEAT-NiTi sample, the topmost porous network surface layer of AEAT-NiTi sample as Fig. 1(d) shows was probably made of sodium titanate [17]. The sodium titanate layer formed during alkaline etching without post heat treatment is too thin to be detected by XRD analysis in this study.

Roughness measurement proved the increased surface roughness after surface modification as SEM results shows and the arithmetic average roughness (R_a) of all studied samples is listed

in Table 1. UFG-NiTi showed slightly higher R_a than CG-NiTi. The R_a of UFG-NiTi was increased significantly by sandblasting (from 0.042 μm to 1.597 μm), and further slightly increased by subsequent acid and alkaline treatment. Fig. 4 shows the contact angle of tested materials. AE-NiTi exhibited highest contact angle, and AEAT-NiTi lowest.

3.2. Corrosion behavior

The potentiodynamic polarization behavior of surface modified UFG-NiTi samples is depicted by polarization curves in Fig. 5(a). Values of i_{corr} , E_{corr} , and E_{pit} extracted from the curves are shown in Table 2. One can see that i_{corr} increased slightly after sandblasting treatment. The i_{corr} value of AEAT-NiTi was the highest among all the studied samples, which means AEAT-NiTi had highest corrosion rate. It corrodes fast once corrosion occurs. The corrosion potential changed with surface modification. The E_{corr} of SB-NiTi and AEAT-NiTi was lower than UFG-NiTi, while AE-NiTi had highest E_{corr} , which indicates UFG-NiTi passivated during acid etching in HF/ HNO_3 solution and had lowest tendency to corrode. Meanwhile, the E_{pit} was increased from 393 mV (SCE) to 704 mV (SCE)

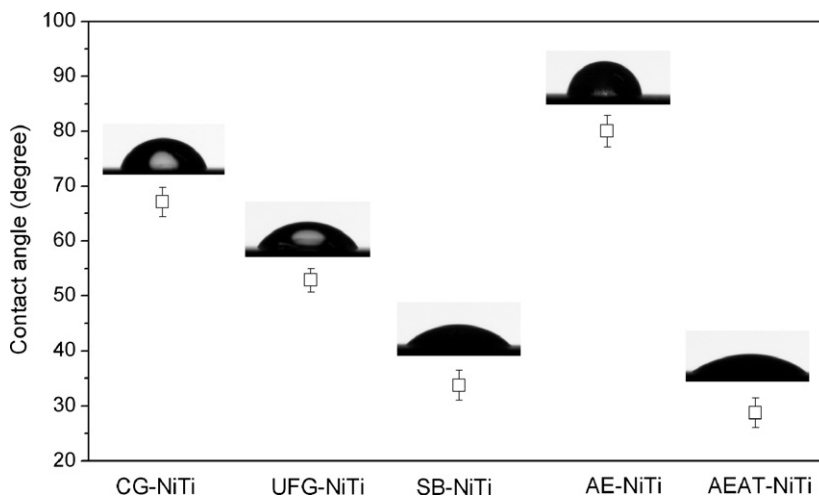


Fig. 4. Contact angle of CG-NiTi and UFG-NiTi with and without surface modification.

Table 1
 Surface roughness of CG-NiTi and UFG-NiTi with and without surface modification.

Samples	CG-NiTi	UFG-NiTi	SB-NiTi	AE-NiTi	AEAT-NiTi
R_a (μm)	0.028 ± 0.007	0.042 ± 0.006	1.597 ± 0.076	1.643 ± 0.030	1.798 ± 0.040

Table 2
 Results of electrochemical parameters.

Samples	E_{corr} (mV (SCE))	i_{corr} ($\mu\text{A}/\text{cm}^2$)	E_{pit} (mV (SCE))	R_p (Ωcm^2)	R_b (Ωcm^2)
CG-NiTi	-294	4.40	534	28.29	6667
UFG-NiTi	-272	3.41	393	28.33	6374
SB-NiTi	-286	4.07	704	30.59	2302
AE-NiTi	-265	3.51	1539	119.7	12410
AEAT-NiTi	-544	44.1	1310	28.38	529.8

with sandblasting and further increased to 1539 mV (SCE) with following acid etching in HF/HNO₃ solution. Thus, AE-NiTi has highest pitting corrosion resistance. Generally, both sandblasting and chemical etching decreased the sensibility of pitting corrosion of NiTi alloy. The new passive layer formation during surface modification and the decrease or elimination of the negative effect of the surface defects and residual stress would account for it. Such behavior was also found by Trépanier [18] that all surface treatments of NiTi such as electropolishing, air aging, heat treatment and passivation in nitric acid solution increased the pitting corrosion resistance. AE-NiTi showed highest E_{corr} and E_{pit} value, which means lowest tendency to corrode or pitting corrode. One reason is that HF/HNO₃ etching removed the residual alumina particles as EDS analysis in Fig. 1 shows. In addition, the decreased sur-

face wettability yielded by HF/HNO₃ etching closely relates to its increased pitting corrosion resistance. Surface wettability of the different samples was determined by measuring the contact angle of deionized water on each sample. Until now, little work has been done to study corrosion resistance from the perspective of wettability. Wang et al. [19] recently found that wetting angles has a strong influence on the corrosion properties of the Zr-BMGs. Hydrophobic TiO₂ coating was reported to exhibit excellent corrosion resistance in chloride containing solution [20]. In this study, results in Fig. 4 show that the contact angle was remarkably large for AE-NiTi, indicating that AE-NiTi was more hydrophobic than SB-NiTi and UFG-NiTi. As known, a hydrophobic surface has lower surface energy than a hydrophilic surface. Thus the surface of AE-NiTi was not as active as UFG-NiTi and got less ion attacks than the active surface with high surface energy. We suggest that taking wettability or surface energy into consideration when exam the anti-corrosion ability of metallic materials as well as many other factors, such as chemical composition, structure, crystallinity and surface defects.

The EIS data acquired at open-circuit potential in SBF are shown in the Nyquist plots in Fig. 5(b). As proposed by Venugopalan [21], the film at Ti alloy surface is composed of a bi-layered oxide consisting of porous outer layer and a barrier inner layer. Thus, considering the surface condition of the ultrafine-grained NiTi with and without surface modification, the obtained Nyquist plots were interpreted in equivalent circuit with a model of $R_s(Q_p(R_p W_p))(Q_b R_b)$ taking into account of diffusion process. In this model, R_p refers to the resistance of the porous layer, and R_b to the resistance of the barrier layer. Two constant-phase elements (Q_p and Q_b) representing the shift from the ideal capacitors were used instead of the capacitances themselves, for simplicity. The fitted curves were also shown in Fig. 5(b). It could be observed that in good agreement between the simulated and experimental data was achieved. It is obvious from Nyquist plots that the diameter of the semicircle for AE-NiTi was biggest than the other studied samples, thus it has highest corrosion resistance. The lowest corrosion resistance was found for AEAT-NiTi which was modified by combined surface treatment of sandblasting with HCl solution etching followed by NaOH solution etching. These results coincided well with the above potentiodynamic polarization.

Among the above three kinds of surface modified samples, AEAT-NiTi shows lowest corrosion potential and highest corrosion density. The i_{corr} of AEAT-NiTi sample is almost twelve times larger than that of untreated UFG-NiTi. There are many factors influencing the corrosion resistance. The sodium titanate layer formed during alkaline treatment on the surface of AEAT-NiTi is less corrosion resistant compared with naturally formed titania layer on UFG-NiTi. Meanwhile, assuming that the corrosion rate remains unchanged during the corrosion process for the porous surface, an increased surface area would result in more ions taking part in the electrochemical process at the metal/solution interface resulting

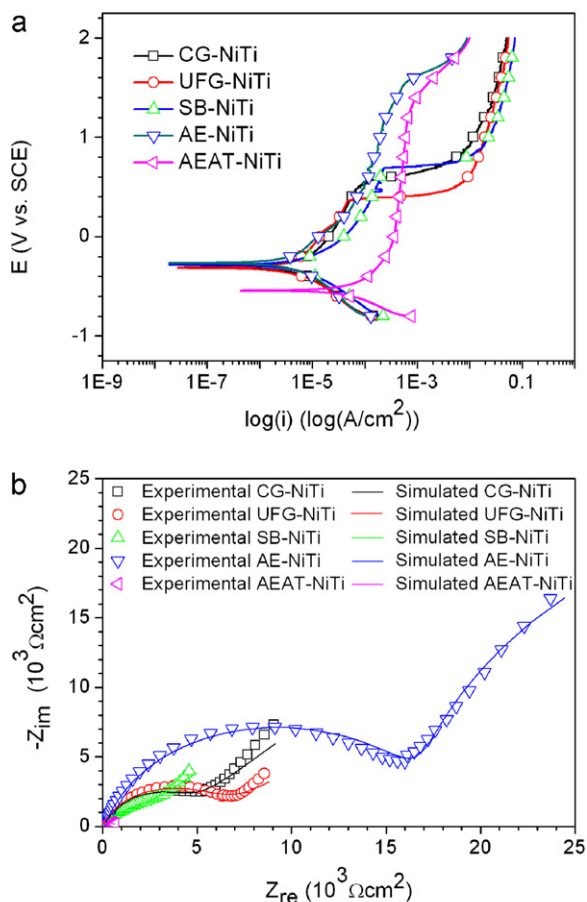


Fig. 5. Potentiodynamic polarization curves (a) and Nyquist impedance diagrams (b) of UFG-NiTi with different surface treatment.

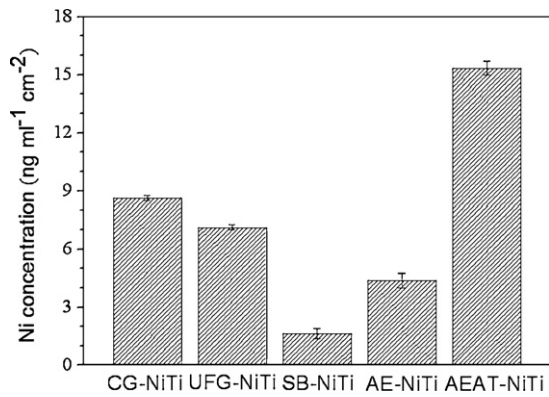


Fig. 6. Release of Ni ions of CG-NiTi and UFG-NiTi with and without surface modification.

in an increase in the current. Thus, one factor leading to the i_{corr} increase of AEAT-NiTi is the increase of surface specific area. Moreover, AEAT-NiTi had a large number of very small size pores (from micrometer to nanometer) among the three kinds of surface modified samples. The small size pores restricted the flow of species and exhausted oxygen supply dissolved in the solution, which also accelerated the corrosion rate. Besides, contrary to AE-NiTi, AEAT-NiTi had rather low water contact angle, close to 30°, which means it being highly hydrophilic. It might be the other factor which leads to its poor corrosion resistance.

Fig. 6 shows the release of nickel ions from experimental NiTi alloys after soaking in SBF for 28 days. UFG-NiTi shows lower amount of Ni ion release compared with CG-NiTi. Sandblasting decreased the releasing rate of Ni ions to a very low level. Although the Ni ion releasing rate of AE-NiTi is higher than that of SB-NiTi, it is significantly lower than that of UFG-NiTi and CG-NiTi. Among all the experimental samples, AEAT-NiTi has the highest Ni ion releasing rate, which indicates that it might be not suitable for implantation.

3.3. Apatite formation and cytocompatibility

The capacity of apatite formation in SBF has been widely used to assess the bioactivity of biomaterials. Such simple test in vitro has been reported to be consistent with the in vivo test. Thus, the bioactivities of the surface modified samples were evaluated in SBF. Fig. 7 shows the morphology and composition of calcium phosphate formed on the surface of NiTi samples for different time. After 3 days immersion in SBF, a complete calcium phosphate layer formed on the surface of AEAT-NiTi (Fig. 7(a)), while only a few calcium phosphate particles deposited on the surface of SB-NiTi (Fig. 7(b)). As arrows in Fig. 7(c) pointed out, few calcium phosphate particles deposited on AE-NiTi. However, after 7 days soaking in SBF, there were many calcium phosphate particles formed and an integrated calcium phosphate layer formed within 14 days soaking (Fig. 7(e) and (f)). Since both morphology and composition are similar to that of apatite [22]. The calcium phosphate on the surface of SB-NiTi is apatite with sodium and magnesium substitution (Fig. 7(f)). The bioactivity tests in SBF show that it took different time for the sur-

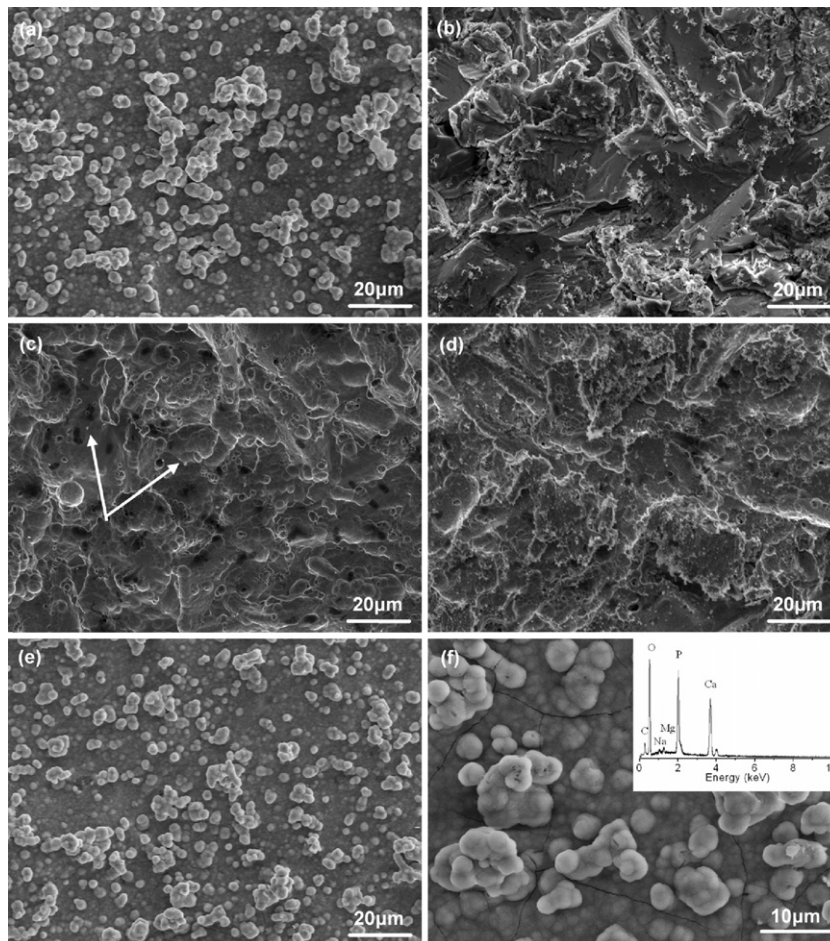


Fig. 7. Apatite SEM morphologies of NiTi samples soaked in SBF for different time: (a) AEAT-NiTi, (b) SB-NiTi, (c) AE-NiTi for 3 days, (d) AE-NiTi for 7 days, (e) AE-NiTi for 14 days, (f) high magnification of (e). EDS spectrum is illustrated in the insets of (f).

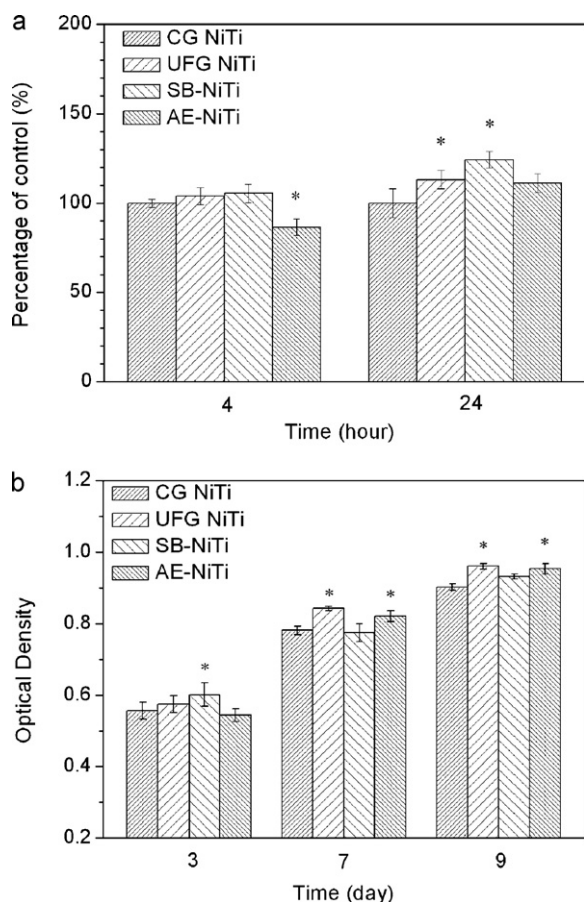


Fig. 8. Cell attachment (a) and proliferation (b) cultured on CG-NiTi, UFG-NiTi, SB-NiTi and AE-NiTi. Columns marked with the * represent significant difference ($P < 0.05$) for UFG-NiTi, SB-NiTi and AE-NiTi groups compared to the CG-NiTi group at each time point.

face modified UFG-NiTi to yield complete apatite layer formation, that is, 3 days for AEAT-NiTi, 7 days for SB-NiTi and 14 days for AE-NiTi. Thus, the ability of apatite formation sequenced as AEAT-NiTi > SB-NiTi > AE-NiTi.

Considering the poor corrosion resistance of AEAT-NiTi, which is not suitable for biomedical application, cell attachment and proliferation behavior were only studied on the other four groups of

samples as shown in Fig. 8. After 4 h culture, the number of cells attached on the CG-NiTi, UFG-NiTi and SB-NiTi was similar, while there were significantly more attached cells on the UFG-NiTi and SB-NiTi than on the CG-NiTi after 24 h culture ($P < 0.05$; Fig. 8(a)). As for AE-NiTi, it had obviously less cells attached than the other studied sample after 4 h cell culture. However, this difference of attached cell numbers between CG UFG and AE-NiTi was reduced after 24 h culture. According to Two-way analysis of variance with Bonferroni's multiple comparison tests, there was no statistical difference between CG-NiTi and AE-NiTi after 24 h culture. The cell proliferation results in Fig. 8(b) show that the number of cells on the SB-NiTi surface was significantly higher than the other tested samples after 3 days culture while more cells were on the surface of UFG-NiTi and AE-NiTi surface at days 7 and 9 of culture.

Fig. 9 shows the morphologies of MG 63 cells cultured on surface modified UFG-NiTi for 4 h and 3 days, and it can be shown that, some of the MG 63 cells showed rounded shapes after 4 h culture (Fig. 9(a), (b) and (d)). These cells landed on the materials later. They were too late to spread and were fixed for observation. However, lots of pseudopodia were observed stretching out. As time went on, the cell started to grow, spread out and proliferate quickly. Fig. 9(e)–(h) shows proliferated cells with health cell morphology.

Surface modification improved cytocompatibility as well as apatite forming ability, but different treatments had different effect on cell behavior at different stage. SB-NiTi with high roughness and wettability increased the cell attachment, while AE-NiTi with distinctly low wettability showed significantly less attached cells after cell culture for 4 h. It seems hydrophobic surface has advantage of improving corrosion resistance but is a disadvantage for initial cell adhesion. However, more cells were on the surface of AE-NiTi than on SB-NiTi after 7 and 9 days culture, which indicates that, compared with sandblasting, treatment of sandblasting with acid etching enhanced cells proliferation. Whether it is because the morphology and geometry differences that AE-NiTi had pores uniformly distributed while SB-NiTi showed irregularly roughened surface or surface wettability difference caused the different proliferation behavior of AE-NiTi and SB-NiTi is still unknown since the effect of surface wettability or surface energy on cell proliferation is unclear. The releasing of alumina particles resided would also be another side effect [23]. Meanwhile, it is found that UFG-NiTi showed slightly faster cell attachment, spreading and proliferation than CG-NiTi, which is consistent with many other published works about enhancement of osteoblast response to ultrafine-grained Ti or NiTi [7,8,10]. The increased amount of surface atoms and grain boundaries and slight increase of surface roughness (Table 1) as

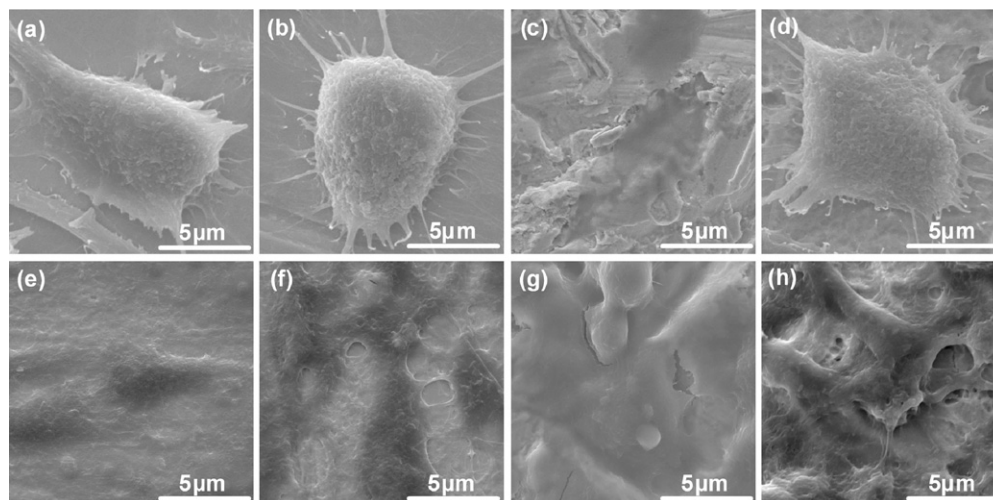


Fig. 9. The morphology of MG63 cells cultured on (a and e) CG-NiTi, (b and f) UFG-NiTi, (c and g) SB-NiTi and (d and h) samples for 4 h (a–d) and 3 days (e–h).

well as decreased water contact angle (Fig. 4) or increased wettability with the refinement of grains are the possible reasons of increased cytocompatibility for UFG-NiTi and possibly suitable for other ultrafine-grained materials.

Therefore, taking account of corrosion resistance, bioactivity and cytocompatibility, sandblasting with HF/HNO₃ solution etching would be a good choice, which decreases the amount of surface nickel content and significantly increases the pitting corrosion resistance, apatite forming ability and cellular response. Although sandblasting with acid etching followed by alkaline treatment yielded a highly bioactive surface, such treatment decreased the corrosion resistance of UFG-NiTi alloy significantly and is not recommended for biomedical implantation.

4. Conclusions

Surface modification of UFG-NiTi with sandblasting increased the pitting corrosion resistance and further increased significantly with following HF/HNO₃ solution etching. The effectiveness of surface treatment on enhancing the bioactivity of UFG-NiTi was in the decreasing order of AEAT-NiTi, SB-NiTi and AE-NiTi. Surface modification improved cytocompatibility of UFG-NiTi for MG63 cells. Sandblasting which increased surface roughness and wettability promoted cell adhesion, while sandblasting plus HF/HNO₃ solution etching increased surface roughness but decreased wettability promoted cell proliferation. In a word, UFG-NiTi with microporous surface yielded by sandblasting and HF/HNO₃ solution etching has the best combination of biocompatibility and pitting corrosion resistance. The three-step treatment of sandblasting with acid etching followed by alkaline treatment severely impaired the corrosion resistance of UFG-NiTi and is not suitable for biomedical application in spite of high surface bioactivity.

Acknowledgements

This work was financially supported by National High Technology Research and Development Program of China (863 Program) under grant number 2011AA030101 and 2011AA030103, NSFC-RFBR joint project (31011120091), National Natural Science Foundation of China (No. 51041004), the Ministry of Science and Technology of China (Project Number 2007CB936103), Research Funds for the Central Universities (PKUJC2009001) and Program for New Century Excellent Talents in University (NCET-07-0033).

References

- [1] R. Valiev, Nanostructuring of metals by severe plastic deformation for advanced properties, *Nat. Mater.* 3 (2004) 511–516.
- [2] S.G. Wang, C.B. Chen, K. Long, H.Y. Yang, F.H. Wang, Z.D. Zhang, Preparation and electrochemical corrosion behavior of bulk nanocrystalline ingot iron in HCl acid solution, *J. Phys. Chem. B* 109 (2005) 2499–2503.
- [3] R.Z. Valiev, A.K. Mukherjee, Nanostructures and unique properties in intermetallics subjected to severe plastic deformation, *Scripta Mater.* 44 (2001) 1747–1750.
- [4] S. Faghihi, A.P. Zhilyaev, J.A. Szpunar, F. Azari, H. Vali, M. Tabrizian, Nanostructuring of a titanium materials by high-pressure torsion improves pre-osteoblast attachment, *Adv. Mater.* 19 (2007) 1069–1073.
- [5] R.Z. Valiev, I.P. Semenova, E. Jakushina, V.V. Latysh, H. Rack, T.C. Lowe, J. Petruželka, L. Dluhoš, D. Hrušák, J. Sochová, Nanostructured SPD processed titanium for medical implants, *Mater. Sci. Forum* 584–586 (2008) 49–54.
- [6] Y. Estrin, E.P. Ivanova, A. Michalska, V.K. Truong, L. Rimma, R. Boyd, Accelerated stem cell attachment to ultrafine grained titanium, *Acta Biomater.* 7 (2) (2011) 900–906.
- [7] Y.T. Zhu, T.C. Lowe, R.Z. Valiev, V.V. Stolyarov, V.V. Latysh, G.J. Raab, Ultrafine-grained titanium for medical implants. US Patent 6399215 (2000).
- [8] F.L. Nie, Y.F. Zheng, Y. Cheng, S.C. Wei, R.Z. Valiev, In vitro corrosion and cytotoxicity on microcrystalline, nanocrystalline and amorphous NiTi alloy fabricated by high pressure torsion, *Mater. Lett.* 64 (2010) 983–986.
- [9] Z.Q. Yao, Y. Ivanisenko, T. Diemant, A. Caron, A. Chuvilil, J.Z. Jiang, R.Z. Valiev, M. Qi, H.J. Fecht, Synthesis and properties of hydroxyapatite-containing porous titania coating on ultrafine-grained titanium by micro-arc oxidation, *Acta Biomater.* 6 (2010) 2816–2825.
- [10] J.W. Park, Y.J. Kim, C.H. Park, D.H. Lee, Y.G. Ko, J.H. Jang, C.S. Lee, Enhanced osteoblast response to an equal channel angular pressing-processed pure titanium substrate with microrough surface topography, *Acta Biomater.* 5 (2009) 3272–3280.
- [11] H. Shao, C. Yu, X. Xu, J. Wang, R. Zhai, Wang, F. X., Influence of Ti nanocrystallization on microstructure, interface bonding, surface energy and blood compatibility of surface TiO₂ films, *Appl. Surf. Sci.* 257 (2010) 1649–1654.
- [12] C.Y. Zheng, F.L. Nie, Y.F. Zheng, Y. Cheng, S.C. Wei, R.Z. Valiev, Enhanced in vitro biocompatibility of ultrafine-grained titanium with hierarchical porous surface, *Appl. Surf. Sci.* 257 (2011) 5634–5640.
- [13] R.D.K. Misra, S.A. Mali, S.S. Nayak, M.C. Somani, L.P. Karjalainen, Favorable surface adhesion response of electrocrystallized nanohydroxyapatite on ultrafine-grained/nanograined austenitic stainless steel, *Scripta Mater.* 59 (2008) 834–837.
- [14] C.Y. Zheng, F.L. Nie, Y.F. Zheng, Y. Cheng, S.C. Wei, L. Ruan, R.Z. Valiev, Enhanced corrosion resistance and cellular behavior of ultrafine-grained biomedical NiTi alloy with a novel SrO–SiO₂–TiO₂ sol–gel coating, *Appl. Surf. Sci.* 257 (2011) 5913–5918.
- [15] T. Kokubo, H. Takadama, How useful is SBF in predicting in vivo bone bioactivity? *Biomaterials* 27 (2006) 2907–2915.
- [16] C.Y. Zheng, S.J. Li, X.J. Tao, Y.L. Hao, R. Yang, Surface modification of Ti–Nb–Zr–Sn alloy by thermal and hydrothermal treatments, *Mater. Sci. Eng. C* 29 (2009) 1245–1251.
- [17] Y. Liu, X. Yang, M. Chen, S. Zhu, Z. Cui, Deposition of bioactive layer on NiTi alloy by chemical treatment, *J. Mater. Sci. Technol.* 18 (2002) 534–537.
- [18] C. Trépanier, M. Tabrizian, L.H. Yahia, L. Bilodeau, D.L. Piron, Effect of modification of oxide layer on NiTi stent corrosion resistance, *J. Biomed. Mater. Res. B* 43 (1998) 433–440.
- [19] Y.B. Wang, H.F. Li, Y.F. Zheng, S.C. Wei, M. Li, Correlation between corrosion performance and surface wettability in ZrTiCuNiBe bulk metallic glasses, *Appl. Phys. Lett.* 96 (2010) 251909.
- [20] R. Rofagha, U. Erb, D. Ostrander, G. Palumbo, K.T. Aust, The effects of grain size and phosphorus on the corrosion of nanocrystalline Ni–P alloys, *Nanostruct. Mater.* 2 (1993) 1–10.
- [21] R. Venugopalan, J.J. Weimer, M.A. George, L.C. Lucas, The effect of nitrogen diffusion hardening on the surface chemistry and scratch resistance of Ti–6Al–4V alloy, *Biomaterials* 21 (2000) 1669–1677.
- [22] M. Wei, H.M. Kim, T. Kokubo, J.H. Evans, Optimising the bioactivity of alkaline-treated titanium alloy, *Mater. Sci. Eng. C* 20 (2002) 125–134.
- [23] M. Rüger, T.J. Gensior, C. Herren, M. von Walter, C. Ocklenburg, R. Marx, H.J. Erli, The removal of Al₂O₃ particles from grit-blasted titanium implant surfaces: effects on biocompatibility, osseointegration and interface strength in vivo, *Acta Biomater.* 6 (2010) 2852–2861.